Molecular Biology of the Cell
Vol. 21, 1850–1863, June 1, 2010

α-Synuclein Delays Endoplasmic Reticulum (ER)-to-Golgi Transport in Mammalian Cells by Antagonizing ER/Golgi SNAREs

Nandhakumar Thayanidhi, Jared R. Helm, Deborah C. Nycz, Marvin Bentley, Yingjian Liang,* and Jesse C. Hay

Division of Biological Sciences and Center for Structural and Functional Neuroscience, University of Montana, Missoula, MT 59812-4824

Submitted September 17, 2009; Revised March 31, 2010; Accepted April 2, 2010
Monitoring Editor: Sean Munro

Toxicity of human α-synuclein when expressed in simple organisms can be suppressed by overexpression of endoplasmic reticulum (ER)-to-Golgi transport machinery, suggesting that inhibition of constitutive secretion represents a fundamental cause of the toxicity. Whether similar inhibition in mammals represents a cause of familial Parkinson's disease has not been established. We tested elements of this hypothesis by expressing human α-synuclein in mammalian kidney and neuroendocrine cells and assessing ER-to-Golgi transport. Overexpression of wild type or the familial disease-associated A53T mutant α-synuclein delayed transport by up to 50%; however, A53T inhibited more potently. The secretory delay occurred at low expression levels and was not accompanied by insoluble α-synuclein aggregates or mistargeting of transport machinery, suggesting a direct action of soluble α-synuclein on trafficking proteins. Co-overexpression of ER/Golgi arginine soluble *N*-ethylmaleimide-sensitive factor attachment protein receptors (R-SNAREs) specifically rescued transport, indicating that α-synuclein antagonizes SNARE function. Ykt6 reversed α-synuclein inhibition much more effectively than sec22b, suggesting a possible neuroprotective role for the enigmatic high expression of ykt6 in neurons. In in vitro reconstitutions, purified α-synuclein A53T protein specifically inhibited COPII vesicle docking and fusion at a pre-Golgi step. Finally, soluble α-synuclein A53T directly bound ER/Golgi SNAREs and inhibited SNARE complex assembly, providing a potential mechanism for toxic effects in the early secretory pathway.

INTRODUCTION

α-Synuclein is a cytosolic neuronal protein whose overexpression or mutation in humans causes Parkinson's disease (PD) and involves the selective death of dopaminergic neurons (Cookson and van der Brug, 2008). α-Synuclein overexpression in cultured cells has been shown to inhibit mitochondrial function, protein synthesis, proteasome function, and exocytosis and to induce the unfolded protein response and oxidative stress (Cookson and van der Brug, 2008). Although any of these effects on key cellular functions could cause toxicity, a central problem in these studies is unraveling which effects are a direct result of α-synuclein protein and which arise as a secondary consequence of its harmful activities. Strategies to ameliorate cellular damage in PD would ideally target disruptive processes most proximal to α-synuclein.

This article was published online ahead of print in *MBoC in Press* (http://www.molbiolcell.org/cgi/doi/10.1091/mbc.E09–09–0801) on April 14, 2010.

* Present address: Department of Psychiatry, New York University School of Medicine, 550 First Ave., New York, NY 10016.

Address correspondence to: Jesse C. Hay (jesse.hay@umontana.edu).

Abbreviations used: α-syn, α-synuclein; ERES, endoplasmic reticulum exit site; NRK, normal rat kidney; PD, Parkinson's disease; SNARE, soluble *N*-ethylmaleimide-sensitive factor attachment protein receptor.

The native function of α-synuclein in neurons is under intense investigation. The endogenous protein is present on the surface of synaptic vesicles in neurons, and its overexpression inhibits vesicle priming for fusion (Fortin *et al.*, 2005; Larsen *et al.*, 2006; Nemani *et al.*, 2010). Gene knockout studies support a required role for the endogenous protein in maintenance of synaptic vesicle pools (Cabin *et al.*, 2002). A positive role as a chaperone for synaptic vesicle transport machinery was suggested by genetic interactions with the cysteine string protein (Chandra *et al.*, 2005). Complicating matters is the observation that α-synuclein is an intrinsically unfolded protein that accumulates in cytoplasmic polyubiquitinated protein aggregates (Cookson and van der Brug, 2008). Whether these insoluble intracellular aggregates are causally related to PD is unclear.

A potential breakthrough in understanding α-synuclein toxicity in PD resulted from a high-copy suppressor screen conducted in yeast (Cooper *et al.*, 2006). α-Synuclein overexpression was found to suppress yeast growth, providing the opportunity to search for genes whose co-overexpression restored viability. Most of the discovered genetic modifiers were trafficking machinery for endoplasmic reticulum (ER)-to-Golgi transport, including a rab protein, COPII coat subunits and regulators, and a soluble *N*-ethylmaleimide-sensitive factor attachment protein receptor (SNARE). The ability of multiple ER-to-Golgi transport proteins to largely reverse the toxicity of α-synuclein overexpression strongly implied that the cellular pathology was primarily related to the actions of α-synuclein on ER-to-Golgi vesicle transport. Indeed, ER-to-Golgi transport was blocked in yeast and

other processes such as oxidative stress, if affected, were either not life-threatening to yeast or were secondary results of the block in vesicle transport. The yeast in which transport was inhibited accumulated massive cytoplasmic aggregates containing α-synuclein, transport vesicles, and most of the cellular pool of ER/Golgi rabs and SNAREs (Gitler *et al*., 2008), suggesting a mechanism involving postbudding depletion of transport machinery from their site of function. A hypothetical mechanism for familial PD was proposed wherein a primary defect in ER-to-Golgi transport could selectively cause dopaminergic neuronal death (Cooper *et al*., 2006; Gitler *et al*., 2008). Inadequate delivery of proteins such as the vesicular monoamine transporter to synaptic sites could allow dopamine and its by-products to accumulate in the synaptic cytoplasm, causing oxidative stress. Thus, the inability to properly compartmentalize dopamine metabolism could selectively kill dopaminergic neurons, although in principle ER-to-Golgi transport would be inhibited in all cells overexpressing α-synuclein. However, the yeast xenogenetic system is a potential concern, and it has remained untested whether α-synuclein targets the mammalian secretory pathway at analogous steps. Furthermore, the role of large α-synuclein aggregates and inclusions such as those that nonselectively consumed yeast rabs and transport vesicles (Gitler *et al*., 2008) is controversial and may represent a downstream consequence as opposed to a cause of α-synuclein toxicity (Cookson and van der Brug, 2008). In addition, many studies of α-synuclein toxicity, including those cited above, use very high overexpression levels that could in principle induce toxic effects unrelated to the development of the human disease.

Here, we document that relatively mild overexpression of human α-synuclein, wild-type or disease-associated mutants, specifically and potently inhibits ER-to-Golgi transport in mammalian cells, and that overexpression of ER-to-Golgi SNAREs reverses this transport inhibition directly, i.e., without affecting α-synuclein expression, localization, aggregation or disposal. α-Synuclein A53T maximally inhibited transport at low expression levels. The inhibition of ER-to-Golgi transport did not involve mistargeting of endogenous transport machinery, for example into α-synuclein-aggregates (Gitler *et al*., 2008). These findings support a direct inhibitory action of monomeric or soluble α-synuclein oligomers on ER/Golgi transport machinery in its unperturbed membrane environment. In support of this hypothesis, purified α-synuclein protein directly inhibited pre-Golgi COPII vesicle docking and fusion in vitro. Finally, purified, soluble, unaggregated α-synuclein A53T protein directly bound ER/Golgi SNAREs and inhibited the in vitro assembly of the fusogenic ER/Golgi SNARE complex. In cells, overexpression of the arginine (R)-SNARE ykt6 conferred more potent resistance to α-synuclein inhibition than the ER/Golgi R-SNARE sec22b.Ykt6 in mammals is expressed at low levels in most cell types and functions in Golgi- and endosome-related membrane fusion steps (Zhang and Hong, 2001; Fukasawa *et al*., 2004; Tai *et al*., 2004). Intriguingly, ykt6 is dramatically overexpressed in neurons and the dopaminergic PC12 cell line (Hasegawa *et al*., 2003) for unknown reasons, where most of the protein seems to be stored in novel cytoplasmic particles (Hasegawa *et al*., 2004). One possibility is that ykt6's unique propensity among SNAREs to confer resistance to secretory insults has a neuroprotective effect, providing a rationale for its enigmatic overexpression in neurons.

MATERIALS AND METHODS

Antibodies and Expression Constructs

Mouse monoclonal anti-myc antibodies were purified from hybridoma 9E10 tissue culture supernatants. Mouse monoclonal anti-human α-synuclein was obtained from BD Biosciences (San Jose, CA; catalog no. 610786). Rabbit polyclonal anti-human α-synuclein antibody was obtained from Sigma-Aldrich (St. Louis, MO; catalog no. S3062). Rabbit polyclonal anti-Golgi phosphoprotein of 130 kDa (GPP130) was obtained from Covance Research Products (Princeton, NJ; catalog no. PRB144C). Mouse monoclonal anti-β-galactosidase (β-gal) antibody was obtained from Developmental Studies Hybridoma Bank (University of Iowa, Iowa City, IA). Rabbit polyclonal anti-rat lysosome-associated membrane protein (LAMP)-1 was obtained from Calbiochem (San Diego, CA; catalog no. 428017). Rabbit polyclonal anti-rab1A was obtained from Santa Cruz Biotechnology (Santa Cruz, CA; catalog no. sc-311). Mouse monoclonal anti-LC3 was from MBL (Nagoya, Japan; catalog no. M152-3). Chicken polyclonal anti-rat ykt6 was developed in our laboratory and described previously (Hasegawa *et al*., 2003, 2004), as were antibodies against sec22b, rbet1, rsly1, p24, and sec31 (Xu *et al*., 2000; Xu and Hay, 2004). Chicken polyclonal anti-rat p115 was a kind gift from Dr. Elizabeth Sztul (University of Alabama-Birmingham, Birmingham, AL). Wild-type α-synuclein and A53T constructs in pcDNA 3.1 were a kind gift from Dr. Diane Hanger (King's College London, United Kingdom). Rat myc-ykt6 and mouse myc-sec22b constructs were described previously (Hasegawa *et al*., 2003, 2004). Residues 710-3755 encoding β-galactosidase in the pSV-β-galactosidase control vector (Promega, Madison, WI; catalog no. E1081) were amplified using specific primers including restriction sites for SacII and XbaI. The polymerase chain reaction (PCR) product was cut using SacII and XbaI and subcloned into SacII/XbaI-digested pcDNA3.1 encoding an N-terminal myc epitope to generate the myc-lacZ construct. Syntaxin 5 small interfering RNA (siRNA) oligonucleotide sequences were a kind gift from Dr. Andrew Peden (Cambridge Institute for Medical Research, Cambridge, United Kingdom).

Transport Assay

Normal rat kidney (NRK) cells were maintained in DMEM high glucose containing 10% fetal calf serum and penicillin-streptomycin. Suspensions of NRK cells were electroporated with 15 μg of α-synuclein DNA construct; for rescue experiments, the α-synuclein construct was coelectroporated with 15 μg of myc-ykt6 or myc-sec22b DNA constructs. Mock-transfected cells were electroporated with no DNA present. After 48 h of protein expression at 37°C, the cells were electroporated a second time with 15 μg of vesicular stomatitis virus-glycoprotein-green fluorescent protein (VSV-G-GFP) DNA construct. They were then grown overnight on poly-L-lysine–coated coverslips at 40°C. For the 0-min time point, coverslips were directly transferred from 40°C to fixative. For other time points, coverslips were transferred from 40°C into six-well chambers containing pre-equilibrated 32°C medium for various intervals and then transferred to fixative. PC12 cells were maintained as described previously (Hasegawa *et al*., 2003) and seeded at 0.5–1.0 × 10^6 cells/well in six-well plates followed by transfection using Lipofectamine 2000 (Invitrogen, Carlsbad, CA) as per manufacturer's instructions. Four micrograms of VSVG-GFP DNA was cotransfected with either 4 μg of α-synuclein A53T DNA, β-gal DNA, or no DNA ("mock") per well for 8 h. The media were then replaced with fresh PC12 media and allowed to grow overnight. After 24 h, the cells were transferred to coverslips in conditioned media and maintained at 40°C for another 24 h. Transport assays were carried out as described for NRK cells.

Immunofluorescence Microscopy

Coverslips were fixed with 4% paraformaldehyde containing 0.1 M sodium phosphate, pH 7.0, for 30 min at room temperature and quenched twice for 10 min with phosphate-buffered saline (PBS) containing 0.1 M glycine. Fixed cells were treated for 15 min at room temperature with permeabilization solution containing 0.4% saponin, 1% bovine serum albumin (BSA), and 2% normal goat serum dissolved in PBS. The cells were then incubated with primary antibodies diluted in permeabilization solution for 1 h at room temperature. Next, coverslips were washed three times with permeabilization solution and incubated 30 min at room temperature with different combinations of fluorescein isothiocyanate (FITC)-, Cy3-, amino-methyl-coumarin-acetate (AMCA)-, and/or Cy5-conjugated anti-mouse, anti-rabbit, or anti-chicken secondary antibodies. After the secondary antibody incubation, coverslips were again washed three times with permeabilization solution and mounted on glass slides using Slow Fade Gold antifade reagent (Invitrogen), and the edges were sealed with nail polish. Slides were analyzed using 40× and 60× objectives on an E800 microscope (Nikon, Tokyo, Japan) with excitation and emission filter wheels (Chroma Technology, Brattleboro, VT), Orca 2 camera (Hamamatsu, Bridgewater, NJ), and Z-drive (Nikon), all automated using OpenLab 5.0 software (Improvision, Coventry, United Kingdom). For transport index assays, the images collected for each field of cells were VSV-G-GFP (FITC filters), α-synuclein (AMCA filters), GPP130 (Cy5 filters), and either ykt6 or sec22b (Cy3 filters).

Image Analysis and Quantitation

Images for quantitation were collected in a consistent manner with regard to cell morphology, protein expression levels, and exposure. After choosing a fixed exposure time for each color channel that would accommodate the majority of cells, we avoided any cell whose intensity values in any color exceeded the saturation value of 16383 on our 14-bit acquisition system. We also avoided capturing cells lacking flat morphology and single, well defined nuclei surrounded on all sides by an expanse of cytoplasm. Only cells exhibiting relatively high synuclein intensities (approximately the top 25%) were selected for all the experiments except where different expression levels of proteins were purposefully used to analyze transport (see Figure 4B). For quantification purposes, a single widefield image plane was collected for each color channel for each field of cells randomly encountered containing at least one qualifying cell. Image deconvolution was not performed. Background in all quantification images was removed by defining a dark extracellular area of the image as zero using the automation tool in OpenLab. To ensure unbiased quantitation, all captured cells meeting the above criteria were assigned numbers that were associated only with the VSV-G-GFP image. Next, the marked VSVG-GFP–expressing cells were coded to mask their identity and isolated from all of the other images that could reveal their condition. After the transport index parameters were determined in OpenLab, the images were uncoded and reassembled with matching images from the same fields. Transport indices were calculated from at least 20 cells per condition.

The Golgi region was defined by GPP130 immunofluorescence: a Golgi mask was created by thresholding the GPP130 image at 25% of its maximum value. This was used to identify the Golgi pixels in the associated VSV-G-GFP image. Transport index was calculated from the VSV-G-GFP image as the maximum pixel intensity within the Golgi region mask divided by the mean pixel intensity in the cell periphery. Maximum intensity was used for the Golgi instead of mean to avoid having to calculate the precise cross-sectional area of the Golgi, which leads to greater variance. The peripheral fluorescence in the denominator of the transport index was derived from a sample of the ER taken by manually drawing an oval-shaped region of interest (ROI) with the long dimension extending from the edge of the nucleus to roughly the edge of the cell; the surface of the nucleus on which the ROI abuts was chosen so as to optimally avoid encompassing or being near any Golgi elements. The mean pixel intensity for this ROI on the VSV-G-GFP image was the denominator of the transport index. Transport index was calculated for each cell separately.

To compare the total protein expression levels of quantitated cells, the boundary of the cell was defined by manually drawing an ROI around the cell on the α-synuclein image. The ROI was then applied to the α-synuclein, VSVG-GFP, ykt6, or sec22b images, and the fluorescence data were collected. Total staining intensity for a protein was calculated as the product of mean intensity and the area of the ROI. In experiments to purposefully correlate transport index with protein expression levels, images were collected of cells having different fluorescence intensity levels by using a single exposure time; after calculation of transport indices as usual, total staining intensity was calculated, and the cells were organized into two or more intensity bins.

To quantify induction of LC3, NRK cells were transfected with the α-synuclein (A53T) construct and allowed to express the protein for 48 h. Serum-starved cells (the positive control for induction) were obtained by growing the cells in serum-free DMEM for 4 h before fixation. Cells were fixed and processed for immunofluorescence using the usual protocol, with rabbit polyclonal anti-α-synuclein antibody (Sigma-Aldrich), mouse monoclonal anti-LC3 antibody, and their respective Cy3- and FITC-conjugated secondary antibodies. Mock and serum-starved cells were chosen at random for image capture. A53T-transfected cells were chosen by looking in the Cy3 channel to find strong A53T-expressing cells. Image stacks containing 21 planes in the FITC channel were taken for each cell in 0.2-μm increments and deconvolved using Huygens software. One image plane near the image center was selected for quantitation. The background in these cells was subtracted by setting a dark extracellular area in the field to zero by using the automation tool in OpenLab software. LC3 objects were identified and counted using a binary mask generated by thresholding LC3 labeling at 4 times the cytosolic background intensity in the cell. Twenty cells were counted in each condition.

Triton X-100 Insolubility Assay

NRK cells were transfected with the α-synuclein A53T DNA construct as usual. After 2 days of protein expression, the cells were harvested in cold lysis buffer (150 mM NaCl, 50 mM Tris, pH 7.6, and 2 mM EDTA, with protease inhibitors) containing 1% Triton X-100. The lysate was mixed end-over-end for 30 min and then centrifuged at 10,000 × *g* for 15 min at 4°C. The detergent-insoluble pellet was then washed twice in PBS and dissolved in SDS sample buffer. The detergent soluble supernatant was briefly sonicated and adjusted to 1× SDS sample buffer. Equal proportions (1%) of detergent-resistant and -soluble fractions were resolved on a 15% acrylamide gel and immunoblotted.

Expression Analysis by Flow Cytometry

NRK cells were electroporated with α-synuclein A53T in pcDNA 3.1 and cells were grown to express the protein for 2 d. Mock-transfected cells were electroporated in the absence of plasmid DNA. Cells were trypsinized, resuspended, and washed three times with PBS. The cells were then fixed, quenched, permeabilized, and immunolabeled as described above for immunofluorescence microscopy except that reagent changes and washes involved centrifugation and resuspension. Secondary antibodies used were FITC-conjugated anti-mouse antibody for detecting α-synuclein and phycoerythrin (PE)-conjugated anti-rabbit antibody for detecting rbet1, membrin, syntaxin 5, and sec22b. Labeled NRK cells were analyzed using an FACSCalibur flow cytometer (BD Biosciences) and FlowJo software (Tree Star, Ashland, OR). Cells were gated consistently on forward and side scatter properties to exclude damaged cells or debris from our data. Labeling with only the secondary antibodies was used as a negative control to ensure that specific labeling for each antigen was present.

Endoglycosidase H (Endo H) Resistance Acquisition Assay

To express the model cargo and potential transport inhibitors with a cotransfection efficiency necessary for analysis in cell lysates, we electroporated NRK cells with constructs for VSV-G-myc and either β-galactosidase, α-synuclein A53T, or empty pcDNA3.1 vector at a 1:2 mass ratio. Unlike in the NRK microscopy assays (see Figures 1–6), we could not introduce the two vectors by using sequential transfections, thus allowing several days of α-synuclein expression (the cotransfection efficiency of that procedure was too low for lysate experiments and VSV-G-myc was too toxic to introduce >24 h before assay). After 24 h postelectroporation at 37°C, we infected the cells with vaccinia virus vTF7 (Fuerst *et al*., 1986; Dascher *et al*., 1995; Xu and Hay, 2004) for 4–6 h, yielding an approximately threefold amplification of β-galactosidase and α-synuclein beyond preinfection levels (data not shown). This amplification was necessary to partially offset the shorter expression time and the less-than-optimal coexpression levels compared with the microscopy experiments, in which NRK cells expressed α-synuclein for 3 d before assay, the cotransfection efficiency of chosen cells was 100%, and only robustly expressing cells were included in the analysis. After shift to 32°C for varying periods, cells were lysed with 0.1 M citrate, pH 5.5 (NaOH), 0.1% SDS, 0.8% β-mercaptoethanol, and protease inhibitors; incubated at 95°C for 3 min; and centrifuged at 100,000 × *g* for 20 min. Thirty microliters of the supernatants was incubated or not with 5 U of endo H (Roche Diagnostics, Indianapolis, IN) for 16–24 h at 37°C before SDS-polyacrylamide gel electrophoresis (PAGE) analysis and immunoblotting using an anti-myc antibody. The endo H-sensitive (G_S) and endo H-resistant (G_R) band ratio was captured in a linear range with an LAS-3000 imager (Fujifilm, Tokyo, Japan) for chemiluminescence and quantitated using ImageGauge software (Fujifilm).

Homotypic COPII Vesicle Fusion Assay

COPII vesicle fusion experiments were carried out as described previously (Xu and Hay, 2004; Bentley *et al*., 2006; Cai *et al*., 2007). In brief, the VSV-G-myc–expressing NRK cells and pulse-radiolabeled VSV-G*-containing cells were permeabilized by scraping with a rubber policeman and then washed and resuspended at ~170 μl/10-cm plate in 50/90 buffer (50 mM HEPES, pH 7.2, 90 mM potassium acetate). A first-stage (vesicle release) incubation to produce enough vesicles for a 24-point fusion assay contained 1.96 ml and consisted of 432 μl of water, 67.5 μl of 0.1 M magnesium acetate, 135 μl of ATP-regenerating system, 40.5 μl of 1 M HEPES, pH 7.2, 270 μl of weak calcium buffer (20 mM HEPES, pH 7.2, 1.8 mM $CaCl_2$, and 5 mM EGTA), 675 μl of dialyzed rat liver cytosol, and 337.5 μl of either of the permeabilized cell populations. After incubation at 32°C for 30 min to allow vesicle release, cells were removed by centrifugation at 4000 × *g* for 1 min followed by 15,000 × *g* for 1 min. The supernatant, which contains released COPII vesicles, was saved. For the second-stage fusion incubations, each reaction totaled 200 μl and contained 72.5 μl of VSV-G-myc vesicles, 72.5 μl of VSV-G* vesicles, and 55 μl of 25/125 buffer or purified test proteins extensively dialyzed in 25/125 buffer. After a 60-min preincubation on ice with these test components, the reactions were incubated at 32°C for 60 min to allow tethering, fusion, and heterotrimerization between VSV-G-myc and VSV-G* vesicles. For measuring heterotrimers, the final vesicle suspensions were supplemented with 2% Triton X-100, incubated with agitation at 4°C for 20 min and then centrifuged at 100,000 × *g* for 30 min. The 100,000 × *g* supernatants containing solubilized VSV-G trimers were then processed for immunoprecipitation by using 5 μg of biotinylated anti-myc antibodies and 5 μl (packed) streptavidin-Sepharose (GE Healthcare, Little Chalfont, Buckinghamshire, United Kingdom). Immunoprecipitates were solubilized in SDS sample buffer, analyzed by SDS-PAGE (8%) and phosphorimaging, and coprecipitated VSV-G* was quantified.

Full-length human α-synuclein A53T was subcloned into pGEX-KG, expressed as a glutathione transferase (GST) fusion protein, purified, and cleaved using a protocol similar to that for GST-rbet1 (Xu *et al*., 2000). This protein was abundant and soluble when expressed at 37°C, and solubility issues were not encountered during purification and storage. For in vitro fusion assays, GST and GST/α-synuclein (syn) A53T test proteins were prepared in the absence of any detergents. GST-α-synuclein was cleaved free of GST with thrombin, which was then deactivated with phenylmethylsulfonyl fluoride before extensive dialysis in 25/125 buffer and assay.

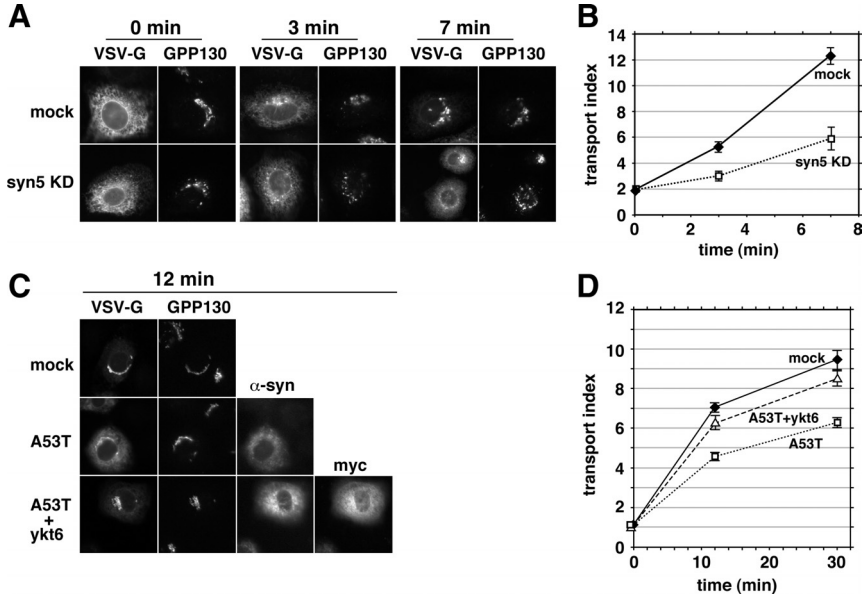

Figure 1. α-Synuclein A53T delays and myc-ykt6 restores ER-to-Golgi Transport. (A) Representative epifluorescent images from several incubation time points displaying VSV-G-GFP and GPP130 in the same cells. The top row of cells were electroporated with buffer only and the bottom row were electroporated with an siRNA for syntaxin 5. (B) Quantitation of transport employing at least 20 randomly chosen cells from each condition (see *Materials and Methods*). (C) Representative images of cells from 12 min at 32°C on separate coverslips singly transfected with VSV-G-GFP (top row), doubly transfected with VSV-G-GFP and α-synuclein A53T (middle row), and triply transfected with VSV-G-GFP, α-synuclein A53T, and myc-ykt6 (bottom row). Golgi staining with GPP130 is shown for each cell. (D) Quantitation of the experiment in C. Error bars represent SEs.

Solution SNARE Assembly and Bead Binding Experiments

Soluble constructs containing the full cytoplasmic domains of syntaxin 5, rbet1 and sec22b, and full-length membrin protein, were expressed in *Escherichia coli*, extracted, renatured, and purified as detailed previously (Xu *et al*., 2000). All purified proteins were dialyzed into buffer A (20 mM HEPES, pH 7.2, 0.15 M KCl, 2 mM EDTA, and 5% glycerol) and stored at −80°C in the presence of 1 mM dithiothreitol, 4 μg/ml aprotinin, 2 μg/ml leupeptin, and 1 μg/ml pepstatin A. For SNARE assembly reactions, 600 pmol of each of the four ER/Golgi SNAREs and a threefold molar excess of purified GST or GST/α-syn A53T were combined to make up 300-μl SNARE assembly reactions with each SNARE at 2 μM, plus 0.1% Triton X-100. After 4 h on ice, the mixture was fractionated on a 24-ml Superdex 200 column, and the fractions were processed as described previously (Xu *et al*., 2000). Because the overexpression studies suggested a directly antagonistic relationship between α-synuclein and R-SNAREs, we preincubated sec22b with GST or GST/α-syn alone on ice before adding the other SNARES. GST and GST/α-syn A53T preparations at the proportions used are shown in Figure 9F.

Bead binding studies also were carried out as detailed previously (Xu *et al*., 2000). For testing SNARE binding to α-synuclein (see Figure 9, A and B), crude bacterial lysates expressing GST or GST-α-syn A53T were mixed with glutathione-Sepharose at 4°C so as to nearly saturate the binding capacity. Then, they were washed extensively and stored as a 50% bead suspension in the refrigerator until use in a binding study. A typical bead binding reaction consisted of 20 μl of 50% glutathione-Sepharose beads containing 124 pmol (620 nM) of immobilized protein and 20–200 pmol (100 nM to1 μM) of soluble binding partners in a final volume of 200 μl also containing 0.1% Triton X-100 and 0.1% BSA. After 1 h at 4°C with constant agitation, beads were washed three times with buffer A plus 0.1% BSA before solubilization of the bound proteins in SDS-PAGE sample buffer. For testing syntaxin 5 binding to membrin beads in the presence or absence of α-synuclein (see Figure 9, C and D), bacterial lysates expressing GST or GST-membrin were prepared as described above. Both the beads and soluble binding partner were preincubated with GST or GST/α-synuclein A53T for 4 h at 4°C. The preincubated beads and soluble binding partner were then combined to a final volume of 200 μl containing 20 μl of 50% beads; 14 μM GST or GST/α-synuclein A53T; and 0.2, 0.5, or 1 μM soluble syntaxin 5 plus detergent and BSA. Syntaxin-5 binding was then determined as described above.

RESULTS

A Morphological ER-to-Golgi Kinetics Assay

To test the hypothesis that α-synuclein inhibits ER-to-Golgi transport in mammalian cells, we developed a fluorescence-based assay for the transport of vesicular stomatitis virus glycoprotein (VSV-G ts045) in intact cells. NRK cells were electroporated with pcDNA3.1-VSV-G-GFP ts045 and incubated at 40°C for 18 h to accumulate cargo in the ER. Coverslips of NRK cells were shifted to 32°C for varying times, and then the cells were fixed and imaged by widefield fluorescence microscopy. In the first experiment, the coverslips were held at 10°C for 1 h immediately preceding the shift to permissive temperature; 10°C allows VSV-G to fold and enter ER exit sites (ERES) but does not allow budding (Mezzacasa and Helenius, 2002). As shown in Figure 1A, the mostly ER pattern of VSV-G-GFP gave way to an increasing concentration in the Golgi over a 7-min time period at 32°C. NRK cells previously electroporated with an siRNA to syntaxin 5, a glutamine $(Q)_A$-SNARE required for ER-to-Golgi transport (Rowe *et al*., 1998; Xu and Hay, 2004), developed little perinuclear concentration, indicating that transport was largely blocked (Figure 1A). Supplemental Figure S1A establishes depletion of syntaxin 5 from the entire cell population. To quantify transport, we calculate a simple transport index ratio that compares fluorescence intensity in the Golgi area to that in the peripheral cytoplasm, representing the ER (see *Materials and Methods*). A transport index of slightly above 1.0 is expected if no accumulation of VSV-G-GFP in the Golgi occurred relative to that in peripheral structures. As shown in Figure 1B, the transport index of VSV-G-GFP rose from ~2 to more than ~12 during 7 min in cells that did not receive siRNA (solid diamonds), but it rose only to ~6 in cells depleted of syntaxin 5 (open squares). Thus, our algorithm reports a highly significant inhibition of transport (70% inhibited at 3 min), after depletion of an established ER/Golgi SNARE. For the remaining experiments, we skipped the 10°C step. As shown in Figure 1D (solid diamonds), the lack of preincubation lowered the starting transport index to ~1.0 and resulted in slightly lower maximal transport values achieved over a longer time course, demonstrating that our method can detect a shift in transport kinetics between two cell populations each capable of full transport. In our standard assay (Figure 1D), the transport index rose nearly 10-fold over a 30-min incubation at 32°C.

α-Synuclein A53T Delays ER-to-Golgi Transport in Mammals

To test whether a PD-associated mutant of α-synuclein affects ER-to-Golgi transport, we electroporated NRK cells with pcDNA3.1 encoding human α-synuclein A53T. Two days later, the cells were electroporated with VSV-G-GFP,

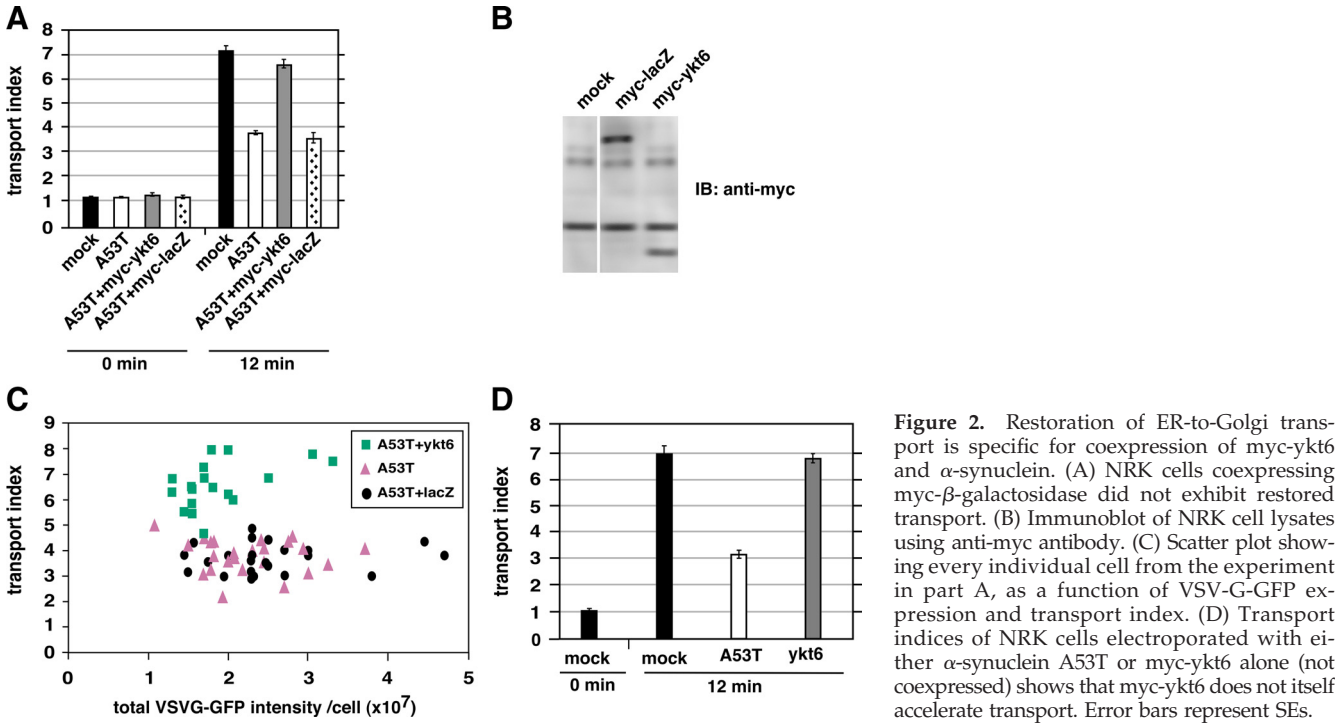

Figure 2. Restoration of ER-to-Golgi transport is specific for coexpression of myc-ykt6 and α-synuclein. (A) NRK cells coexpressing myc-β-galactosidase did not exhibit restored transport. (B) Immunoblot of NRK cell lysates using anti-myc antibody. (C) Scatter plot showing every individual cell from the experiment in part A, as a function of VSV-G-GFP expression and transport index. (D) Transport indices of NRK cells electroporated with either α-synuclein A53T or myc-ykt6 alone (not coexpressed) shows that myc-ykt6 does not itself accelerate transport. Error bars represent SEs.

and the transport assay was performed. As shown in Figure 1C, cells expressing α-synuclein (middle row) displayed less VSV-G-GFP in the Golgi area and retained greater fluorescence in the periphery compared with mock-electroporated cells (top row). As shown in Figure 1D (solid diamonds vs. open squares), the transport index was inhibited by ~40% after 12 min. We also examined the individual intensity parameters that make up the transport index, and we found that α-synuclein A53T inhibited Golgi as well as enhanced peripheral fluorescence (Supplemental Figure S1B), as expected. This eliminates most potential artifacts whereby Golgi or cell size/shape could affect transport index. We noted no cytopathic effects of A53T expression by using the pcDNA3.1 vector for several days. α-Synuclein expression in these studies is relatively low. The immunoblot in Supplemental Figure S1C demonstrates that our transiently transfected NRK cells express ~80% more α-synuclein than present in a comparable protein load of total rat brain lysate. Given our transfection efficiency of ~40%, we estimate that transfected cells express α-synuclein approximately threefold higher than the average cell in a rat brain.

Ykt6 Coexpression Partially Restores Transport

If the inhibition was a direct result of interference with ER/Golgi transport machinery, then overexpression of ER/Golgi machinery might rescue transport. Ykt6p was the only SNARE multicopy suppressor of α-synuclein A53T toxicity in yeast (Cooper *et al.*, 2006). pcDNA3.1 encoding rat myc-ykt6 was coelectroporated with α-synuclein A53T and evaluated using the transport assay. As shown in Figure 1C, bottom row, cells expressing both α-synuclein A53T and myc-ykt6 had similar VSVG-GFP fluorescence to cells lacking α-synuclein A53T (top row, mock). The transport index was ~70% restored in this experiment (Figure 1D); however, the degree of restoration in other experiments varied between 50 and 80% of mock values. Analysis of the individual intensity parameters revealed that ykt6 coexpression increased fluorescence in the Golgi as well as decreased peripheral fluorescence (Supplemental Figure S1B).

We wondered whether coexpression of myc-ykt6 might influence the expression of α-synuclein A53T to lower its toxicity. First, we created an analogous pcDNA3.1 construct encoding myc-β-galactosidase. Coexpression of this construct with α-synuclein A53T, in contrast to myc-ykt6, was found to have no affect on transport index (Figure 2A). Myc-ykt6 and myc-β-galactosidase were expressed at roughly comparable levels according to immunoblotting using anti-myc antibody (Figure 2B). Restoration is thus specific to myc-ykt6. Furthermore, any affects of myc-ykt6 on total α-synuclein expression, as measured by staining intensity, do not account for its restoration of transport (Figure 3B; described below). Another possibility was that ykt6 coexpression might affect the VSV-G-GFP expression and that VSV-G-GFP load affects the transport index. As shown in Figure 2C, myc-ykt6–expressing cells' transport indices were higher over the entire range of VSV-G-GFP. Finally, we wondered whether ykt6 coexpression might generally accelerate ER-to-Golgi transport as opposed to specifically restore. As shown in Figure 2D, myc-ykt6 expression by itself did not significantly affect transport kinetics. We conclude that ykt6 specifically restores ER-to-Golgi transport to α-synuclein A53T-intoxicated cells, independently of affects it may have on α-synuclein and VSV-G-GFP expression patterns.

Sec22b Restores Transport but Less Effectively Than ykt6

In nonneuronal cells, ykt6 is required for transport between the Golgi and endosome (Tai *et al.*, 2004), intra-Golgi transport (Fukasawa *et al.*, 2004), and a late step in ER-to-Golgi transport (Zhang and Hong, 2001). Blockage of the ykt6-dependent step(s) in the biosynthetic secretory pathway results in VSV-G concentration at the Golgi and concomitant depletion from the periphery (Zhang and Hong, 2001). Hence, our transport index would not report a block at the

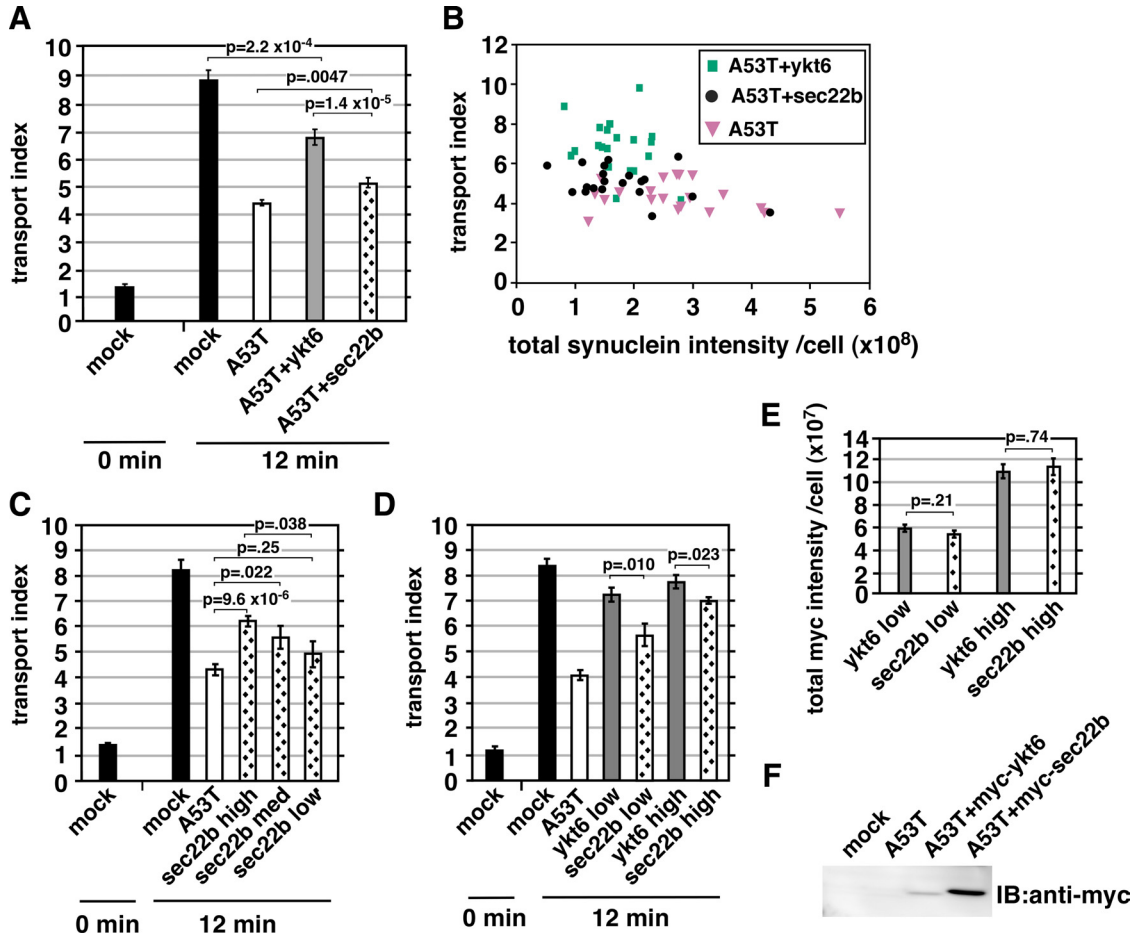

Figure 3. Ykt6 rescues transport more potently than sec22b. (A) Comparison of transport rescue by myc-sec22b and myc-ykt6. (B) Scatter plot showing every cell from the experiment in A, as a function of total cellular α-synuclein A53T staining intensity and transport index. (C) A separate experiment from part A, in which a wide intensity range of myc-sec22b coexpressing cells was imaged, binned according to anti-myc intensity, and transport indices calculated. (D) Another experiment in which anti-myc staining intensities were binned and transport indices plotted for myc-ykt6 and myc-sec22b coexpressing cells. (E) Total anti-myc staining intensities for the bins of cells analyzed in D. (F) Anti-myc immunoblot of NRK cell lysates of duplicate coverslips to those analyzed in D and E. The statistical significance of differences between the indicated mean transport indices are reported as p values from a two-tailed Student's *t* test. Error bars represent SEs.

ykt6-dependent step and α-synuclein A53T, which causes VSV-G to fail to concentrate at the Golgi (Figure 1), must inhibit at earlier step(s) in ER-to-Golgi transport. Early membrane fusion steps in ER-to-Golgi transport are mediated by a quaternary SNARE complex composed of syntaxin 5, membrin, rbet1, and sec22b (Rowe *et al*., 1998; Xu *et al*., 2000; Xu and Hay, 2004). Sec22b is the closest paralogue of ykt6; both are R-SNAREs that fill the structural role of VAMP in SNARE bundles (Hay, 2001) and possess longin domains serving targeting/regulatory functions (Rossi *et al*., 2004). In yeast, loss of *SEC22* can be compensated for by *YKT6* overexpression (Liu and Barlowe, 2002). We coelectroporated NRK cells with α-synuclein A53T together with either myc-sec22b or myc-ykt6 in pcDNA3.1 and compared restoration. As shown in Figure 3A, myc-sec22b restored transport approximately half as well as myc-ykt6. We wondered whether either coexpression construct affected α-synuclein A53T expression and whether this could explain their differing abilities to rescue. As shown in Figure 3B, in any given synuclein staining intensity range, ykt6-cotransfected cells displayed higher transport indices. In this experiment, the imaged cells exhibited ~75% more total anti-myc staining in the myc-sec22b population than in the myc-ykt6 population (data not shown). One possibility was that myc-ykt6 restores transport significantly more potently than myc-sec22b; alternatively, myc-sec22b might inhibit transport at high levels of expression but potently restore transport only when expressed at low levels. We therefore imaged an experiment over a wide range of myc-sec22b expression levels, including some low expressers that would have been avoided above. As shown in Figure 3C, when all of the cells were binned into low, medium, and high expression of myc-sec22b based upon total anti-myc staining intensity, increasing myc-sec22b expression correlated with higher restoration of transport, reaching a maximum at ~50% restoration in the highest expressing population. We conclude that myc-sec22b progressively restored transport in a dose-dependent manner. To directly compare myc-sec22b and myc-ykt6 rescue abilities semiquantitatively, we performed another experiment and imaged cells coexpressing α-synuclein A53T and myc-ykt6 or myc-sec22b over widely overlapping anti-myc staining intensities. In Figure 3D, the anti-myc total staining intensity exhibited by myc-ykt6 and myc-sec22b is segregated into "low" and "high" bins. The mean staining intensities were nearly identical for the two constructs in each bin (Figure 3E). However, in either the low- or high-

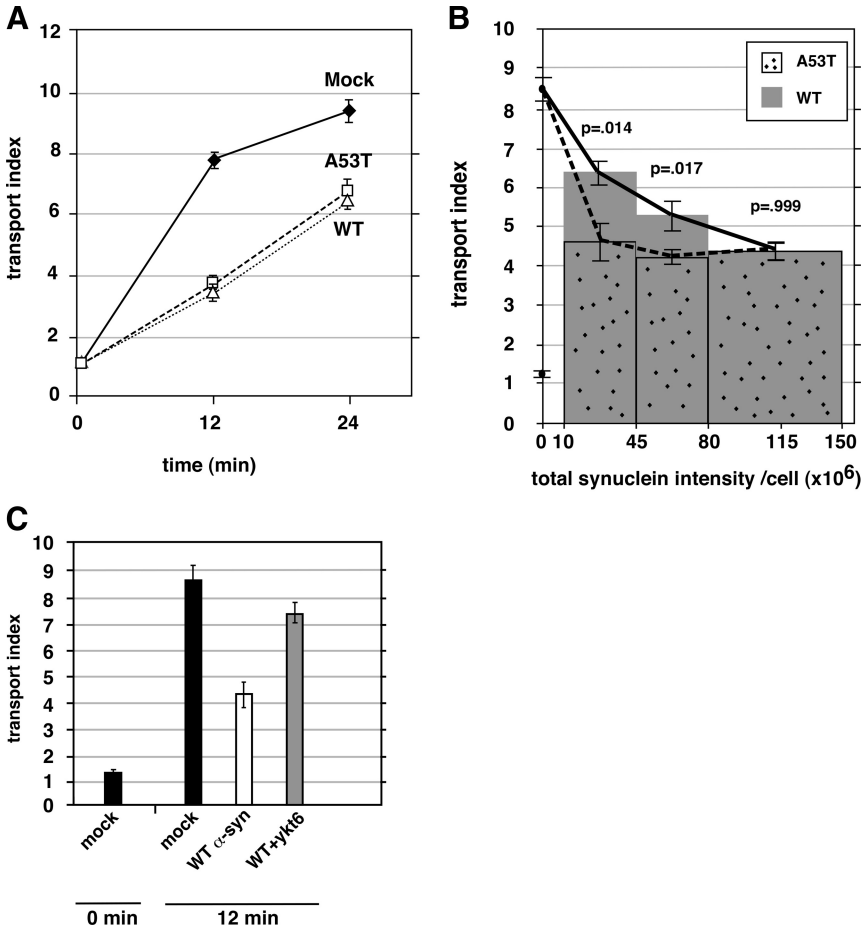

Figure 4. Wild-type α-synuclein delays transport to the same degree, but less potently than A53T. (A) Time course of ER-to-Golgi transport in NRK cells electroporated with wild-type or A53T α-synuclein. Only cells showing strong (approx. top quartile) anti-α-synuclein staining were imaged. (B) A separate experiment in which a wider range of anti-α-synuclein staining intensities were imaged, cells were separated into intensity bins as shown on the *x*-axis, and their transport indices plotted. Both the 12-min and 0-min timepoints are plotted for mock-transfected cells along the y-axis (values of ~8.5 and ~1.2, respectively). (C) Coexpression of myc-ykt6 partially restores transport inhibition caused by wild-type α-synuclein. In some instances, the statistical significance of differences between the indicated mean transport indices are reported as p values from a two-tailed Student's *t* test. Error bars represent SEs.

intensity bin, myc-ykt6 restored transport to a greater degree than myc-sec22b. Importantly, myc-ykt6 restored transport almost equally well in the high and low bin, whereas myc-sec22b restored transport significantly more in the higher bin. Although ykt6 and sec22b share the same domain structure, we could not be certain that the two proteins performed equally for immunostaining. However, immunoblots on the SDS-denatured antigens should provide a more direct comparison. As shown in Figure 3F, when parallel coverslips from this experiment were lysed and immunoblotted, it seemed that myc-sec22b was expressed at least fivefold higher than myc-ykt6, implying that the immunofluorescence signal overestimates myc-ykt6 expression relative to myc-sec22b; in other words, myc-ykt6 is even more relatively potent compared with myc-sec22b than implied in Figure 3D. We conclude that myc-ykt6 restores transport significantly more potently than myc-sec22b, even though the transport inhibition seems to involve sec22b-dependent stage(s) in ER-to-Golgi transport.

Wild-Type α-Synuclein Inhibits Transport Less Potently

PD can be caused by a dominant mutation or by overexpression of the wild-type allele (Cookson and van der Brug, 2008). Thus, if the inhibition of ER-to-Golgi transport is a fundamental cause of PD, we would predict that wild-type α-synuclein should exhibit the same inhibitory properties, but only at higher concentrations. We electroporated NRK cells with A53T or wild-type α-synuclein and tested transport kinetics. As shown in Figure 4A, when using our typical selection criteria, we detected no difference between the transport kinetics of wild-type– and A53T-expressing cells; both were delayed ≥50%. We wondered, however, whether the inhibition of transport may have already reached a maximal value. To examine this, we purposefully imaged cells expressing very wide ranges of α-synuclein expression, including the lowest expressing cells we could confidently qualify as transfected, and we binned cells according to their synuclein staining intensity. As shown in Figure 4B, lower expression levels of wild-type α-synuclein were associated with minimal inhibition of transport and the degree of inhibition increased with increasing staining intensity. However, α-synuclein A53T inhibited almost as completely at low as at high expression levels, indicating that this construct affects the ER/Golgi transport machinery more potently than the wild type. Note that many α-synuclein A53T-transfected cells, perhaps even the majority, fell below the lowest intensity bin in Figure 4B; if we had been able to confidently assign these cells as transfected and obtain transport values, we expect we would also have seen a dose-dependent titration, but left-shifted relative to wild type. As shown in Figure 4C, inhibition of transport by high levels of wild-type α-synuclein were rescued by coexpression with ykt6, to a similar degree as inhibition by A53T (Figures 1–3).

Inhibition Does Not Involve Mistargeting nor Instability of Transport Machinery

In yeast overexpressing α-synuclein A53T, large aggregates formed containing α-synuclein, ER-derived vesicles, endog-

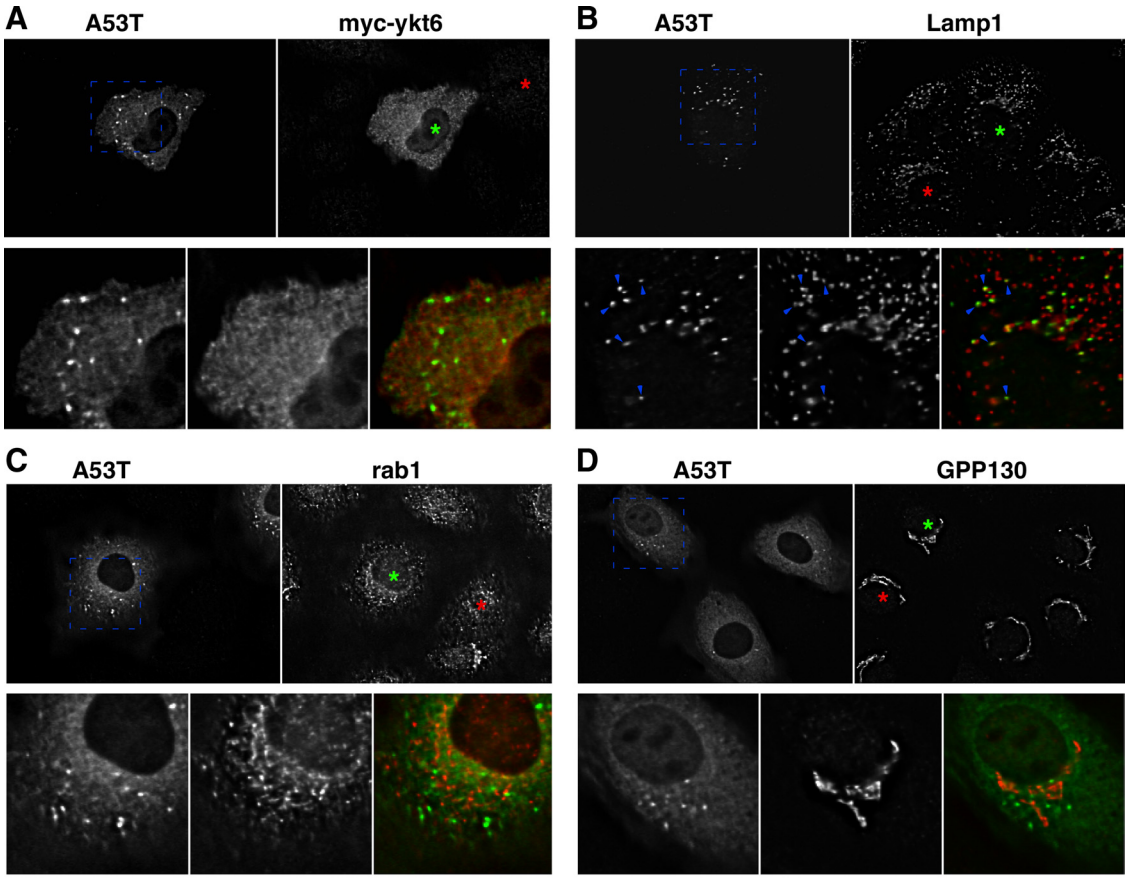

Figure 5. Subcellular distributions of α-synuclein A53T, coexpressed myc-ykt6, and the unperturbed endogenous cellular transport machinery. (A) Comparison between α-synuclein A53T and myc-ykt6 staining patterns. (B) Comparison of α-synuclein A53T and endogenous LAMP-1. Blue arrowheads highlight a few of the α-synuclein-positive particles that are positive for LAMP-1. (C) Comparison of α-synuclein A53T and endogenous rab1. (D) Comparison of α-synuclein A53T and endogenous GPP130. In each block shown, green asterisks mark the nucleus of an α-synuclein A53T-expressing cell and red asterisks mark the nucleus of an untransfected cell for comparison. Shown are individual focal planes of deconvolved wide-field images. (E) A53T-transfected NRK cells were extracted with cold 1% Triton X-100 and centrifuged at 10,000 × *g* for 15 min to generate a supernatant and pellet. Equal proportions of these fractions were analyzed by SDS-PAGE and immunoblotting for α-synuclein and caveolin, a protein known to be in detergent-resistant membrane domains.

enous ER/Golgi SNAREs and rabs (Gitler *et al.*, 2008), suggesting a mechanism whereby transport machinery and secretory membranes could be depleted and their functions' disrupted. In NRK cells, α-synuclein A53T exhibited punctate structures as well as diffuse cytosolic staining (Figure 5, A–D). The diffuse cytosolic staining varied in intensity relative to the particles. We do not know whether the particulate α-synuclein is present in protein aggregates. However, all α-synuclein immunofluorescence staining was extracted by 0.05% Triton X-100 treatment before fixation (data not shown), and all α-synuclein protein detectable by immunoblotting was found in the soluble fraction of a cold 1% Triton X-100 total extract of NRK cells (Figure 5E). These results indicate that any aggregation, if present, had not yet progressed to detergent resistance. The lack of large or detergent-insoluble aggregates under our conditions indicates that such species are not required to achieve the 40–50% delay in ER-to-Golgi transport.

The majority of α-synuclein A53T particles were positive for LAMP-1, but only a fraction of LAMP-1–containing particles were positive for synuclein, consistent with the α-synuclein being associated with specialized lysosome-associated organelles, e.g., autolysosomes (Figure 5B). We noted an amplification of synuclein particles upon addition of the autophagy inhibitor 3-methyl adenine (3-MA; Supplemental Figure S2, A and B) (Webb *et al.*, 2003), consistent with a relationship of the α-synuclein particles to the autophagic degradation pathway. In addition, transfection with α-synuclein A53T caused induction of the early autophagosome marker LC3 (Supplemental Figure S2C). In contrast, LC3 was only rarely present on the structures positive for A53T by immunofluorescence (Supplemental Figure S3D). One possibility consistent with the data are that degradation of α-synuclein occurs by a macroautophagic pathway but that α-synuclein only becomes concentrated significantly in autolysosomes, a membranous structure no longer positive

for LC3 (Kabeya *et al.*, 2000; Tanida *et al.*, 2004). However, we also cannot eliminate the possibility of chaperone-mediated autophagy (Vogiatzi *et al.*, 2008); the exact route(s) by which α-synuclein concentrates in LAMP-positive structures under our conditions is still an open question.

It was important to establish whether rescue of ER-to-Golgi transport by coexpression with myc-ykt6 affected the targeting of α-synuclein. As shown in Figure 5A, myc-ykt6 in NRK cells exhibited a largely cytoplasmic localization. In the cells overexpressing myc-ykt6, no change in the abundance or size of α-synuclein particles was apparent compared with cells only overexpressing A53T (Figure 5, A vs. B–D). Together with the analysis indicating that myc-ykt6 overexpression did not restore transport by altering α-synuclein expression level (Figure 3B), these findings suggest that myc-ykt6 does not restore transport by modulating α-synuclein A53T expression, aggregation, or disposal and favors a direct mode of function whereby a small portion of myc-ykt6 inserts into quasi-functional secretory membranes and restores function by acting as a SNARE.

Under the conditions in which α-synuclein inhibited ER-to-Golgi transport, we observed no colocalization of endogenous SNAREs with the α-synuclein A53T particles, as exhibited by the distributions of sec22b (Supplemental Figure S3A) and rbet1 (data not shown). In contrast to the situation in yeast (Gitler *et al.*, 2008), the distribution of the ER-to-Golgi rab1A protein was unchanged by α-synuclein A53T expression (Figure 5C, compare rab1A distribution in cells marked with red vs. green asterisks), and the rab was not detectable in the α-synuclein particles (Figure 5C, merged panel). Furthermore, the Golgi structure remained compact: we saw no trend toward disruption of the GPP130, p115, or p24 patterns in α-synuclein A53T-overexpressing cells (Figure 5D and Supplemental S3, C and D), in contrast to the Golgi dispersal caused by knockdown of syntaxin 5 (Figure 1A) and viral overexpression of A53T (Gosavi *et al.*, 2002). The previously observed Golgi disruption must therefore have been a downstream consequence rather than a primary cause of traffic disruptions. Finally, ERES marked by sec31 were not altered and sec31 was not present in synuclein particles (Supplemental Figure S3B). Because we never noted colocalization between α-synuclein A53T particles and endogenous ER/Golgi transport machinery, it seems likely that the soluble form of α-synuclein A53T is responsible for the inhibition. Furthermore, we conclude that α-synuclein A53T inhibited the transport machinery in situ and did not involve depletion, mistargeting, nor co-aggregation of transport machinery with the inhibitor.

The antagonistic relationship between A53T and ER/Golgi SNAREs led us to question whether A53T altered SNARE expression levels in intoxicated cells. Although no obvious effects on expression were noticed in the localization studies described above for sec22b and rbet1, we examined expression levels comprehensively for all four ER/Golgi SNAREs by using intracellular immunofluorescence labeling quantified by flow cytometry. As shown in Figure 6, A–D, there was no significant change in sec22b, rbet1, syntaxin 5, or membrin labeling intensity upon expression of A53T, even in cells expressing high levels of the offensive protein. The geometric mean labeling intensity was in fact slightly *higher* for all four SNAREs in transfected cells compared with the non-transfected cells in the same population. However, this very small nonspecific increase in SNARE expression also can be observed in control GFP transfections (data not shown), presumably because there is a slight positive correlation between individual cells' robustness of general protein expression and their transfectability. We conclude that the effect of α-synuclein on ER-to-Golgi transport is not due to changes in ER/Golgi SNARE localization, expression, or stability during the time frame of our experiments.

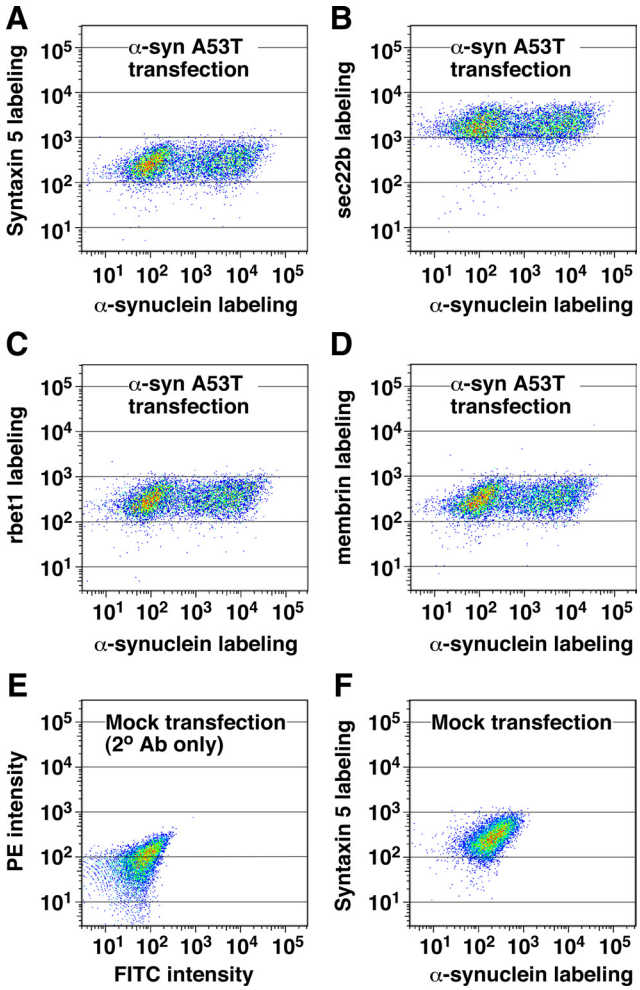

Figure 6. α-Synuclein A53T overexpression does not significantly affect the expression of ER/Golgi SNAREs. Electroporated NRK cells were allowed to express the α-synuclein A53T construct for 2 d before fixation, permeabilization, and immunofluorescence labeling of α-synuclein (with FITC) and each ER/Golgi SNARE (with PE). Labeled cell suspensions were analyzed by flow cytometry. Dot plots display relationship between α-syn A53T labeling and labeling for syntaxin 5 (A), sec22b (B), rbet1 (C), and membrin (D), where the frequency of cells with similar labeling intensities is indicated by color warmth. (E) Mock-transfected cells in which primary antibodies were omitted. (F) Mock-transfected cells labeled with anti-α-synuclein and anti-syntaxin 5 antibodies.

α-Synuclein A53T Inhibits ER-to-Golgi Transport in Neuroendocrine Cells

To test whether α-synuclein A53T overexpression would inhibit ER-to-Golgi transport in cells with a more neuronal phenotype, we applied the same transport assay to PC12 cells, a rat dopaminergic neuroendocrine cell line frequently used in studies of α-synuclein toxicity (Cookson and van der Brug, 2008, and references therein). Chromaffin cells highly express endogenous α-synuclein, whereas the chromaffin derivative PC12 cell line expresses much lower levels (Larsen *et al.*, 2006). As shown qualitatively in Figure 7A, VSV-G-GFP in mock-transfected cells had transitioned from a

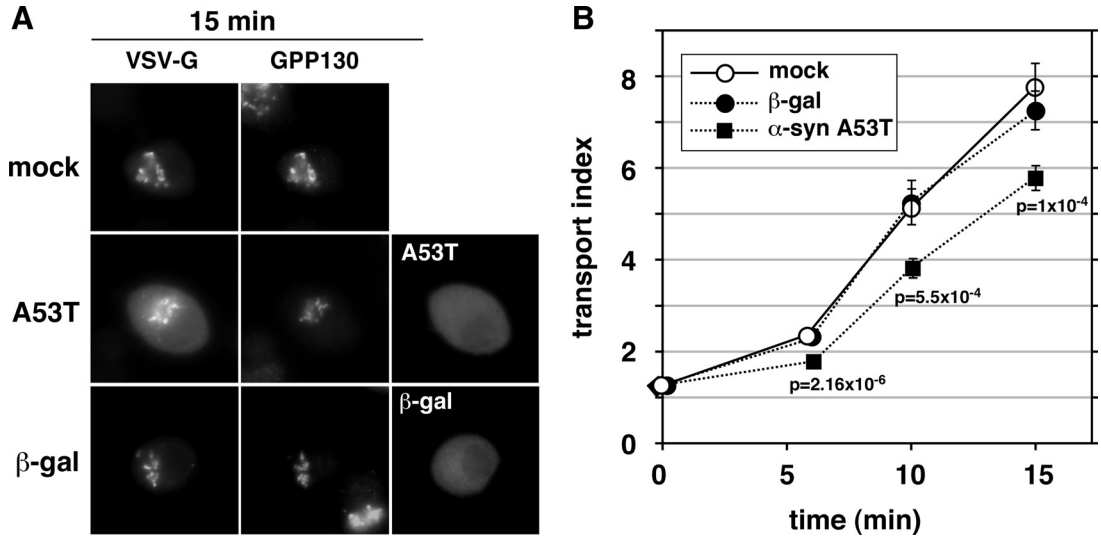

Figure 7. α-Synuclein expression retards ER-to-Golgi transport in neuroendocrine PC12 cells. (A) Representative epifluorescent images from 15 min at 32°C, displaying VSV-G-GFP, GPP130, and either α-synuclein A53T or β-gal driven by pcDNA3.1 transfection. (B) Quantitation of transport employing at least 20 randomly chosen cells from each condition (see *Materials and Methods*). Bars represent SEs and are shown only when exceeding symbol size. The statistical significance of differences between the A53T and mock transport indices at the indicated time points are reported as p values from a two-tailed Student's *t* test.

primarily peripheral ER localization at 40°C to a punctate juxtanuclear localization that coincided with a Golgi marker by 15 min of incubation at 32°C. Furthermore, a similar transition was observed in PC12 cells overexpressing β-galactosidase. In contrast, PC12 cells overexpressing α-synuclein A53T showed relatively less accumulation of VSV-G-GFP in Golgi elements and a greater retention of fluorescence in the periphery. Quantitation of the transport index from PC12 cells randomly chosen from these populations is shown in Figure 7B. In mock- and β-galactosidase–transfected cells, the transport index rose from ~1 to ~8 in 15 min at 32°C. In α-synuclein A53T-transfected cells, however, there was an ~30% inhibition of transport, such that a transport index of ~6 was reached in the same incubation time. The ~30% retardation of transport by α-synuclein was highly statistically significant at the three time points tested. These results demonstrate that α-synuclein A53T inhibition of ER-to-Golgi transport is a feature of neuroendocrine cells and is therefore not unique to nonneuronal cells. In contrast, nonneuronal cells such as NRK may represent a sensitized system for α-synuclein intoxication of the secretory pathway because the smaller degree of inhibition in PC12 cells, 30% as opposed to 50%, indicates that PC12 cells may possess factors or mechanisms that naturally guard against α-synuclein. One of these factors may be ykt6; ykt6 is expressed at particularly high levels in PC12 cells and neurons (Hasegawa *et al*., 2003), and we have shown it to be protective against α-synuclein in NRK cells (Figures 1–3).

α-Synuclein A53T Directly Inhibits ER-to-Golgi Transport by Blocking COPII Vesicle Tethering and Fusion at a Pre-Golgi Step

To further establish the effects of α-synuclein expression on early secretory traffic, we first confirmed the morphological effects (Figures 1–7) in transfected cells by monitoring the rate of transition of VSV-G-myc from its endo H-sensitive to its endo H-resistant form. Due to technical limitations (see *Materials and Methods* for details), we changed our transfection conditions; both VSV-G-myc and A53T (or β-gal or vector only) were introduced in a single electroporation just 24 h before the transport assay and the test protein expression was then amplified approximately threefold by using a vaccinia virus vector encoding T7 RNA polymerase. Shift from 40 to 32°C resulted in increasing conversion from G_S to G_R VSV-G-myc, with complete conversion by 45 min (data not shown). As seen in Figure 8A, A53T caused a trend toward specific inhibition of conversion by 20 min and a specific 23% inhibition of conversion by 30 min of transport, relative to β-gal and vector controls. An example anti-VSV-G-myc blot is shown in Supplemental Figure S4. Although smaller in magnitude, these results confirm the more sensitive morphological assay (which by nature involves 100% cotransfection and only includes cells that express A53T for several days), demonstrating a delay in ER-to-Golgi transport in the presence of α-synuclein A53T.

There are numerous steps where α-synuclein could inhibit VSV-G-myc transport before the mannosidase II modification that imparts endo H resistance. Due to the functional antagonization of ER/Golgi SNAREs by α-synuclein (Figures 1–5), we explored whether at least part of the effects of A53T on transport could be due to a direct effect on SNARE-dependent docking and fusion. ER-to-Golgi cargo transport must involve at least two membrane fusions: one fusion to transfer cargo from COPII vesicles into vesicular tubular clusters (VTCs) in the periphery of the cell and a second fusion to transfer cargo from Golgi-centric VTCs into the *cis*-Golgi (or alternatively to create the *cis*-Golgi de novo). COPII vesicles in vitro contain all components necessary for homotypic tethering and fusion to form nascent VTCs (Xu and Hay, 2004; Bentley *et al*., 2006). Thus, homotypic COPII vesicle fusion seems to represent at least one pre-Golgi membrane fusion contributing to VTC biogenesis and anterograde transport. We used an established cell-free reconstitution of homotypic COPII vesicle fusion (Xu and Hay, 2004; Bentley *et al*., 2006; Yu *et al*., 2006; Cai *et al*., 2007) to generate pre-Golgi intermediates resembling cellular VTCs. Membrane fusion and contents mixing is scored biochemically by the heterotrimerization of radioactive VSV-G* with

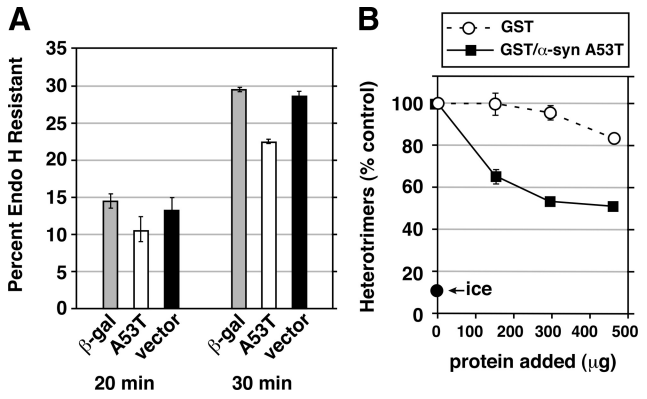

Figure 8. (A) α-Synuclein inhibits transport before cargo modification by mannosidase II. NRK cells were electroporated with VSV-G-myc DNA together with a construct for either β-galactosidase, α-synuclein A53T, or pcDNA3.1 vector alone. After 24 h, the cells were infected with vaccinia virus vTF7 for 6 h at 40°C to amplify expression (see *Materials and Methods*). Cells were either lysed directly (data not shown) or shifted to 32°C for 20, 30, or 40 (data not shown) minutes before lysis, digestion with endoglycosidase H, and immunoblotting with anti-myc to detect VSV-G-myc. Histograms show G_R as a percentage of $G_S + G_R$. Error bars show SE of duplicate gels run on the same cell extracts. The same trends were observed in a completely separate experiment with multiple time points. Supplemental Figure S4 shows one of the immunoblots from which the data were quantified. (B) α-Synuclein A53T directly inhibits COPII vesicle fusion to form pre-Golgi intermediates. Homotypic COPII vesicle fusion measured using the in vitro VSV-G heterotrimer cargo mixing assay. Purified proteins were added after vesicle budding and were incubated with the budded vesicles for 1 h before a 1 h fusion reaction at 32°C. "Ice" indicates heterotrimer signal obtained when the budded vesicles were mixed but left on ice during the fusion incubation. Fusion assay data are presented as means of duplicate determinations with error bars representing SE where larger than symbol size.

nonradioactive VSV-G-myc present initially in distinct COPII vesicle populations. Heterotrimers are easily assayed by detergent solubilization of vesicles, immunoprecipitation using anti-myc antibodies and autoradiography to detect the radioactive subunits (Xu and Hay, 2004). As shown in Figure 8B, purified bacterially expressed GST/α-synuclein A53T (see Figure 9F for a gel on the protein preparations used) inhibited heterotrimer formation, whereas a preparation of GST purified in parallel exhibited only a slight nonspecific inhibition at the highest doses. Equal total protein amounts were compared, which better accounts for nonspecific effects; the molar concentration of α-synuclein at its 153-μg dose is ~19 μM. Thus, the inhibition occurs in a range compatible with the physiological concentration of an abundant cytosolic protein. Interestingly, the inhibition is maximal at ~50%, reminiscent of the incomplete inhibition of ER/Golgi transport, suggesting perhaps that the fusion machinery may be only partially inhibited by α-synuclein or sensitive during only one phase of its life cycle. These results establish a direct effect of α-synuclein protein on the tethering/fusion machinery and suggest that COPII vesicle docking and fusion is at least one of the steps inhibited during A53T transfection experiments. However, it does not rule out that other transport subreactions also could be directly or indirectly affected.

α-Synuclein A53T Directly Binds ER/Golgi SNAREs and Impairs Their Interactions

One potential mechanism for the functional antagonization of SNAREs by α-synuclein would involve a direct interaction of the proteins. α-Synuclein, like unassembled SNARE motifs, is a notably unstructured protein (Cookson and van der Brug, 2008), which could easily lead to promiscuous interactions and/or binding-induced deleterious structuring of the SNARE motifs. Therefore, we preloaded bacterially expressed GST-α-syn A53T fusion protein or control GST onto glutathione-Sepharose beads and tested the beads' ability to capture and pull down the individual soluble SNAREs. To increase the chances of detecting weak or transient binding, each soluble SNARE was tested at concentrations ranging up to and exceeding that at which nonspecific binding to GST beads was observed. As shown in Figure 9A, top two panels, and quantified in Figure 9B, both membrin and syntaxin 5 were captured on GST-α-syn A53T beads at lower input concentrations and to a greater extent than on GST beads, demonstrating a direct protein interaction with α-syn A53T. However, consistent with an inability to detect solution-stable complexes (see below), these interactions were not as robust as we have observed among ER/Golgi SNAREs using the same binding technique (Xu *et al.*, 2000). Alternatively, we did not observe above-background interactions between GST-α-syn A53T and rbet1 (Figure 9A, bottom). Unfortunately, sec22b binds Sepharose beads erratically in binding studies, making a positive outcome possible only in cases of very strong specific binding. The erratic nonspecific binding to beads made it impossible to determine whether weak binding was present (data not shown). For the bead binding studies, consistent recovery of beads and loading of samples is demonstrated in Supplemental Figure S5A by ponceau staining of the same blot used in the immunoblot analysis. Thus, at least a subset of the ER/Golgi SNAREs, including membrin and syntaxin 5, directly interact with α-syn A53T, providing a potential basis for functional antagonization.

To test whether α-synuclein would impair membrin and syntaxin 5 binding activities, we performed binary bead binding studies between these two SNAREs in the presence or absence of soluble α-synuclein. As shown in Figure 9C, left three lanes on the top panel, increasing soluble syntaxin 5 input led to increased retention of syntaxin 5 on GST-membrin beads. However, in the presence of soluble α-synuclein, the same concentrations of soluble syntaxin 5 led to significantly less binding to membrin (Figure 9C, top blot, right three lanes). The presence of soluble α-synuclein A53T did not affect general recovery or solubility of syntaxin 5, because the syntaxin 5 present in supernatants were virtually indistinguishable (Figure 9C, bottom blot). Addition of soluble GST and/or GST/α-synuclein A53T did not affect the amount of GST-membrin immobilized on the recovered beads as indicated by ponceau staining of the blot (Supplemental Figure S5B). Quantification of two identical experiments, including control binding to GST beads, is shown in Figure 9D. From the quantification, it can be seen that α-synuclein reduced syntaxin 5–membrin binary interactions by approximately half. Formation of the physiological, fusogenic SNARE complex involving syntaxin 5, membrin, rbet1, and sec22b involves simultaneous interactions between each one of the ER/Golgi SNAREs with the other three. Partial suppression of several binary interactions each involving syntaxin 5 and membrin could result in a dramatic reduction in the yield of quaternary complex, causing a drastic affect of α-synuclein A53T on *trans*-SNARE complex assembly.

α-Synuclein A53T Impairs SNARE 4-Helix Bundle Formation

To test the possibility that α-synuclein might dramatically inhibit formation of the ER/Golgi quaternary SNARE complex, we used an established SNARE complex assembly

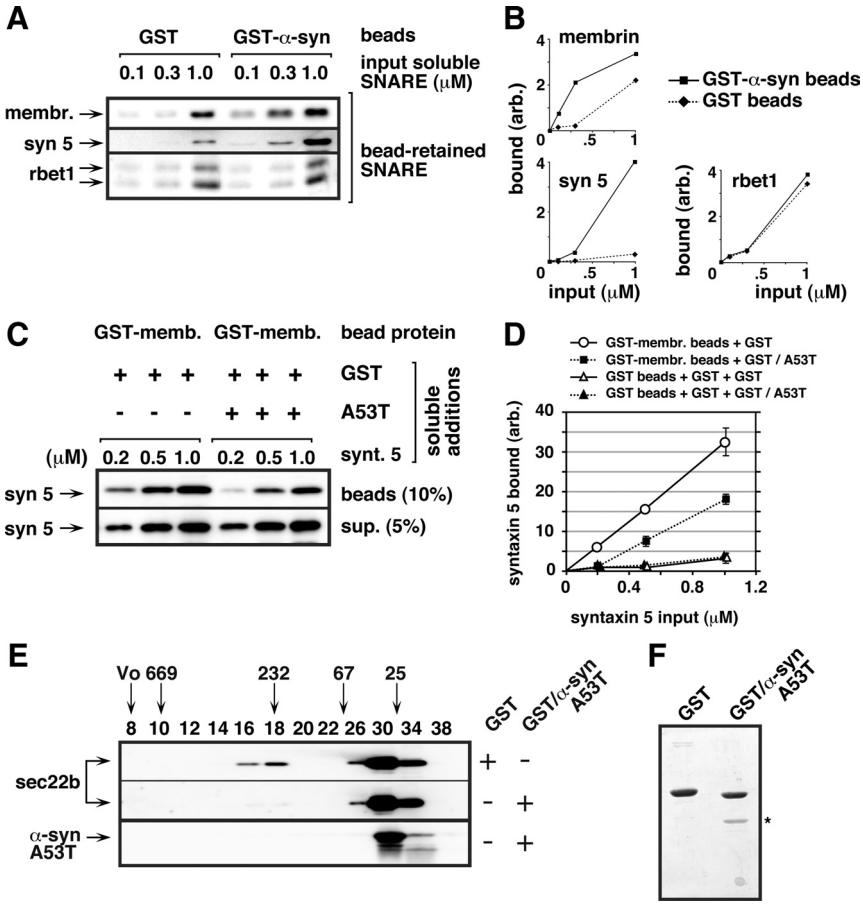

Figure 9. Soluble α-synuclein A53T protein directly binds ER/Golgi SNAREs and inhibits 4-helix bundle assembly in vitro. (A) Glutathione beads preloaded with GST or GST-α-syn A53T were incubated with one of three concentrations of each individual purified, soluble SNARE as indicated along the top edge of the top panel (18 binding reactions in total). Beads were washed extensively with buffer and then analyzed by SDS-PAGE, ponceau staining, and immunoblotting for bead-retained SNAREs using the antibodies listed along the left edge. Ponceau staining for the same set of blots is shown in Supplemental Figure S5A. (B) Quantitation of the binding experiment from A. (C) Glutathione beads preloaded with GST-membrin were incubated with the soluble proteins listed above the blots (see *Materials and Methods* for detailed conditions). After a 1-h binding incubation, beads were sedimented and washed extensively. The presence of syntaxin 5 was determined by quantitative immunoblotting of the washed beads (top blot) and the supernatant from the first centrifugation (bottom blot). (D) Quantification of bead-bound syntaxin 5 from two experiments like that shown in C. Binding of syntaxin 5 to control GST beads is also included, but for simplicity was not shown in C. Error bars indicate SE where exceeding symbol size. Ponceau stain of the blot in C can be found in Supplemental Figure S5B. (E) Purified soluble sec22b, syntaxin 5, membrin, and rbet1 were coincubated with either purified soluble GST or GST/α-syn A53T, as indicated with "+" and "−" along right edge. After a 4-h ice incubation with all five purified proteins (see *Materials and Methods* for detailed conditions), the mixture was fractionated by Superdex 200 chromatography. Selected column fractions, listed along the top edge, were analyzed by SDS-PAGE and immunoblotting using the antibodies listed along the left edge. Positions of globular proteins of known molecular size or blue dextran ("Vo") are indicated with arrows above the fraction numbers. (F) Coomassie-stained SDS-PAGE gel analysis of GST and GST/α-syn A53T preparations in the same proportions used in the preincubations in parts C and E. An asterisk marks the α-syn A53T protein band.

assay involving purified, soluble versions of syntaxin 5, membrin, rbet1, and sec22b (Xu *et al*., 2000; Joglekar *et al*., 2003; Joglekar and Hay, 2005). In this assay, the four soluble SNARE constructs are incubated together on ice to allow assembly into a SNARE complex and then gel filtered to separate assembled species from remaining individual components. The ER/Golgi quaternary complex elutes in fractions corresponding to globular markers of~250 kDa and contains all of the SNARE motifs of the input SNAREs in the stoichiometry 1Qa:1Qb:1Qc:1R. Although the calculated molecular mass of the quaternary complex is 85 kDa, its oligomerization state, overall rod-like shape, and an unknown amount of bound detergent contribute to its elution in higher molecular mass gel filtration fractions (Xu *et al*., 2000). Formation of four-helix bundles with this structural organization is highly conserved among SNAREs and seems to represent the thermodynamic engine for membrane fusion. Indeed, formation of the yeast version of the ER/Golgi quaternary complex causes lipid and content mixing of purified synthetic vesicles (McNew *et al*., 2000). In vitro, sec22b will not assemble into any solution-stable species *except* the quaternary complex containing all four ER/Golgi SNAREs (Xu *et al*., 2000). Due to this remarkable cooperativity, assembly of the full ER/Golgi quaternary complex can be monitored in gel filtration simply by monitoring the elution of a single protein—sec22b—as it shifts from its monomer peak at ~25 kDa (fractions 26–34) to the quaternary complex peak at ~225 kDa (fractions 16–18). All of the sec22b in fractions 16–18 is part of a quaternary complex containing all four ER/Golgi SNAREs (Xu *et al*., 2000).

GST or GST/α-syn A53T were mixed in approximately threefold molar excess with the purified ER/Golgi SNAREs. SNARE complex assembly was allowed to proceed, in the presence of GST or GST/α-syn, for 4 h, and then the protein mixtures were gel filtered by Superdex 200 chromatography. As shown in Figure 9E, top, a portion of sec22b was able to assemble with the other SNAREs into the quaternary SNARE complex present in fractions 16–18, after a control preincubation with GST. The relatively small proportion of sec22b assembled was not significantly different from when GST was omitted (data not shown) and is typical for the time, temperature, and SNARE preparations used (Xu *et al*., 2000; Joglekar *et al*., 2003; Joglekar and Hay, 2005). Strikingly, we found that the inclusion of GST/α-syn A53Twith the SNAREs blocked elution of sec22b in fractions 16–18 (Figure 9E, second panel). Conversely, the amount of total sec22b recovered in the column fractions did not change significantly from the control, and sec22b eluted overwhelmingly in the monomer fractions (26–34), demonstrating that α-syn A53T did not seem to cause aggregation, sequestration into nonproductive complexes, nor significant loss of sec22b during our analysis. We conclude that α-syn

A53T blocked quaternary complex formation and caused sec22b to remain unassembled. These results were consistent over numerous repetitions and with several batches of proteins (data not shown). Supplemental Figure S5C shows subsaturating exposures of immunoblots of the soluble protein mixtures injected onto gel filtration in Figure 9E. Although there are relatively small variations in soluble protein after the incubations that could be due to α-syn A53T (e.g., by effects on adsorption of proteins to plastic surfaces), these small differences could not explain the decisive and selective effects seen on quaternary complex formation.

The α-syn A53T present in the SNARE mixture eluted at a low molecular mass (Figure 9E, bottom, fraction 30), consistent with it being a monomer of an unstructured protein with a slightly larger tumbling radius than its molecular mass of 14.5 kDa would predict. No aggregated α-syn A53T in the void (fractions 6–8) nor solution-stable α-syn-SNARE complexes were apparent by gel filtration. We conclude that soluble, low-molecular-mass α-syn A53T prevented ER/Golgi quaternary SNARE complex assembly via a direct effect on SNARE interactions. Solution binding studies, especially involving the greater dilution and time during a gel filtration step, present more stringent conditions for binding than the GST pull downs where fusion proteins are highly concentrated on a bead surface. The SNARE-α–synuclein interactions detected in bead-biding studies in Figure 9, A and B, may have been too weak or transient to be evident by gel filtration, whereas their effects on assembly of the quaternary SNARE complex, a solution-stable species, were clearly apparent.

DISCUSSION

Despite important differences in the role of aggregation phenomena between the yeast and our studies, our data are consistent with the recently proposed hypothesis that inhibition of ER/Golgi transport is the initiating and most fundamental cellular toxicity of α-synuclein (Cooper *et al*., 2006; Hamamichi *et al*., 2008). That α-synuclein protein acts directly on the transport machinery is supported by multiple observations of this study: 1) α-syn A53T maximally inhibits transport at low expression levels and in the absence of any apparent cytopathic effects, detergent-insoluble aggregates, mistargeting or coaggregation of transport machinery; 2) coexpression of α-syn A53T with ER/Golgi SNAREs nearly completely overcomes the transport delay, but these SNAREs do not in and of themselves accelerate ER-to-Golgi transport, nor alter α-synuclein expression, aggregation or disposal, indicating that transport restoration occurs by replacement of SNAREs incapacitated by α-synuclein; 3) soluble α-syn A53T protein directly inhibits SNARE-dependent COPII vesicle docking and fusion at a pre-Golgi step in vitro; 4) soluble α-syn A53T binds ER/Golgi SNAREs and inhibits formation of the fusogenic 4-helix bundle required for the earliest step(s) in the secretory pathway.

Although our data are compatible with a toxicity-initiating role for the inhibition of ER/Golgi transport in PD (Cooper *et al*., 2006), many other cytotoxicities (Cookson and van der Brug, 2008) may subsequently occur as domino effects—some of which may actually be more disruptive to neurons. Consistent with our mild overexpression conditions, we noted no cytopathic effects of A53T expression using the pcDNA3.1 vector for several days. On the other hand, relatively mild secretory delays could cause tissue- and cell type-specific diseases where highly efficient ER/Golgi transport is needed for extracellular matrix deposition (Townley *et al*., 2008) or compartmentation of dopamine (Cooper *et al*., 2006). Furthermore, even if delayed ER/Golgi transport does not itself harm cells, the resulting unfolded protein response would eventually cause toxicity (Sugeno *et al*., 2008).

Although the results in Figure 9E clearly show that α-synuclein A53T directly inhibited ER/Golgi quaternary SNARE complex assembly, they do not distinguish which specific step in assembly was inhibited and which particular assembly intermediates failed to form. The inhibition of SNARE complex assembly seen in Figure 9E could be caused by weak or transient α-synuclein interactions with one, two, or more of the four ER/Golgi SNAREs. α-synuclein A53T may transiently bind the SNARE motifs to perturb their structure and/or compete with other SNAREs for binding. No evidence for a SNARE sequestering or coaggregation mechanism for the α-syn A53T effect was found, because in the gel filtration experiments, α-synuclein always behaved as a low molecular weight species with a sharp elution, even in the presence of the inhibited ER/Golgi SNAREs (Figure 9E, bottom).

A previous report found that the endogenous function of α-synuclein in the synapse may be to cooperate with the synaptic vesicle chaperone cysteine string protein to somehow protect or maintain SNARE activity (Chandra *et al*., 2005). Interestingly, our studies indicate that excess or mutant α-synuclein has the opposite effect on the ER/Golgi SNAREs. We can only speculate that in the synapse, there are other cellular factors, one possibility being cysteine string protein, that allowα-synuclein to carry out a positive function in membrane docking and/or fusion. In the early secretory pathway, in the absence of synaptic co-chaperones, α-synuclein may exhibit an activity that slows the analogous step(s) in docking and fusion. Thus, normal neurons expressing α-synuclein may be in a delicate balance between supporting synaptic function and slowing the biosynthetic secretory pathway through disruption of ER/Golgi SNAREs. Overexpression or mutation of α-synuclein may simply amplify the negative features of this normal cellular trade-off.

Other reports from the synapse argue for a regulatory role of α-synuclein upstream of docking in the maintenance of the readily releasable pool of synaptic vesicles (Fortin *et al*., 2005; Larsen *et al*., 2006). Too much α-synuclein would lead to a decreased vesicle reclustering after endocytosis and decreased releasable vesicle pool (Nemani *et al*., 2010). This inhibitory role of α-synuclein overexpression could be completely independent of it's effects on SNAREs and the biosynthetic secretory pathway; alternatively, one could imagine how it could arise as an indirect consequence of altered biosynthetic transport of membrane proteins to the plasma membrane or endosomes. For example, due to decreased biosynthetic delivery and/or replenishment rates, key synaptic vesicle trafficking machinery may be present at lower abundance in the synapse, rendering the reclustering of vesicles less efficient. Though a few synaptic proteins were examined and found to be present at wild-type levels (Nemani *et al*., 2010), the variable trafficking itineraries, recycling and turnover rates of distinct membrane proteins in the synapse makes it nearly impossible to exclude that slowed ER-to-Golgi transport altered the abundance of key proteins affecting vesicle replenishment.

What properties of ykt6 might make it a more potent suppressor of the transport defect? One possibility is that because ykt6 normally participates in several membrane fusion complexes, it possesses a greater functional flexibility that makes it a superior suppressor of ER-to-Golgi transport, which involves multiple distinct fusion complexes. Another

possibility is that because ykt6 may be able to target to sites of function directly from the cytosol (Fukasawa *et al*., 2004), rather than by transport through the secretory pathway, it may be better suited to restoring function to membranes that would be otherwise unreachable–in other words, ykt6 could be acting as a SNARE smoke jumper. Although our results do not prove that ykt6 expression is naturally elevated in neurons because α-synuclein is present in those tissues, it does suggest at least one side benefit of this overexpression—a more robust early secretory pathway.

ACKNOWLEDGMENTS

We thank Dr. Brian Storrie for starting us down the path of image quantification, Dr. Scott Wetzel for comments on our quantification scheme and for help with flow cytometry, Pam Shaw (University of Montana Fluorescence Cytometry Core), and Dr. Meg Trahey for comments on the manuscript. This work was supported by National Institutes of Health (NIH) grants GM-59378 and MH-68524 (to J.C.H.) and NIH Center for Biomedical Research Excellence grant RR-015583.

REFERENCES

Bentley, M., Liang, Y., Mullen, K., Xu, D., Sztul, E., and Hay, J. C. (2006). SNARE status regulates tether recruitment and function in homotypic COPII vesicle fusion. J. Biol. Chem. *281*, 38825–38833.

Cabin, D. E., *et al*. (2002). Synaptic vesicle depletion correlates with attenuated synaptic responses to prolonged repetitive stimulation in mice lacking alpha-synuclein. J. Neurosci. *22*, 8797–8807.

Cai, H., Yu, S., Menon, S., Cai, Y., Lazarova, D., Fu, C., Reinisch, K., Hay, J. C., and Ferro-Novick, S. (2007). TRAPPI tethers COPII vesicles by binding the coat subunit Sec23. Nature *445*, 941–944.

Chandra, S., Gallardo, G., Fernández-Chacón, R., Schlüter, O. M., and Südhof, T. C. (2005). alpha-Synuclein cooperates with CSPalpha in preventing neurodegeneration. Cell *123*, 383–396.

Cookson, M. R., and van der Brug, M. (2008). Cell systems and the toxic mechanism(s) of alpha-synuclein. Exp. Neurol. *209*, 5–11.

Cooper, A. A., *et al*. (2006). alpha-Synuclein blocks ER-Golgi traffic and Rab1 rescues neuron loss in Parkinson's models. Science *313*, 324–328.

Dascher, C., Tisdale, E. J., and Balch, W. E. (1995). Transient expression of small GTPases to study protein transport along secretory pathway in vivo using recombinant T7 vaccinia virus system. Methods Enzymol. *257*, 165–173.

Fortin, D. L., Nemani, V. M., Voglmaier, S. M., Anthony, M. D., Ryan, T. A., and Edwards, R. H. (2005). Neural activity controls the synaptic accumulation of alpha-synuclein. J. Neurosci. *25*, 10913–10921.

Fuerst, T. R., Niles, E. G., Studier, F. W., and Moss, B. (1986). Eukaryotic transient-expression system based on recombinant vaccinia virus that synthesizes bacteriophage T7 RNA polymerase. Proc. Natl. Acad. Sci. USA *83*, 8122–8126.

Fukasawa, M., Varlamov, O., Eng, W. S., Söllner, T. H., and Rothman, J. E. (2004). Localization and activity of the SNARE Ykt6 determined by its regulatory domain and palmitoylation. Proc. Natl. Acad. Sci. USA *101*, 4815–4820.

Gitler, A. D., *et al*. (2008). The Parkinson's disease protein alpha-synuclein disrupts cellular Rab homeostasis. Proc. Natl. Acad. Sci. USA *105*, 145–150.

Gosavi, N., Lee, H. J., Lee, J. S., Patel, S., and Lee, S. J. (2002). Golgi fragmentation occurs in the cells with prefibrillar alpha-synuclein aggregates and precedes the formation of fibrillar inclusion. J. Biol. Chem. *277*, 48984–48992.

Hamamichi, S., Rivas, R. N., Knight, A. L., Cao, S., Caldwell, K. A., and Caldwell, G. A. (2008). Hypothesis-based RNAi screening identifies neuroprotective genes in a Parkinson's disease model. Proc. Natl. Acad. Sci. USA *105*, 728–733.

Hasegawa, H., Yang, Z., Oltedal, L., Davanger, S., and Hay, J. C. (2004). Intramolecular protein-protein and protein-lipid interactions control the conformation and subcellular targeting of neuronal Ykt6. J. Cell Sci. *117*, 4495–4508.

Hasegawa, H., Zinsser, S., Rhee, Y., Vik-Mo, E. O., Davanger, S., and Hay, J. C. (2003). Mammalian ykt6 is a neuronal SNARE targeted to a specialized compartment by its profilin-like amino terminal domain. Mol. Biol. Cell *14*, 698–720.

Hay, J. C. (2001). SNARE complex structure and function. Exp. Cell Res. *271*, 10–21.

Joglekar, A. P., and Hay, J. C. (2005). Evidence for regulation of ER/Golgi SNARE complex formation by hsc70 chaperones. Eur. J. Cell Biol. *84*, 529–542.

Joglekar, A. P., Xu, D., Rigotti, D. J., Fairman, R., and Hay, J. C. (2003). The SNARE motif contributes to rbet1 intracellular targeting and dynamics independently of SNARE interactions. J. Biol. Chem. *278*, 14121–14133.

Kabeya, Y., Mizushima, N., Ueno, T., Yamamoto, A., Kirisako, T., Noda, T., Kominami, E., Ohsumi, Y., and Yoshimori, T. (2000). LC3, a mammalian homologue of yeast Apg8p, is localized in autophagosome membranes after processing. EMBO J. *19*, 5720–5728.

Larsen, K. E., *et al*. (2006). Alpha-synuclein overexpression in PC12 and chromaffin cells impairs catecholamine release by interfering with a late step in exocytosis. J. Neurosci. *26*, 11915–11922.

Liu, Y., and Barlowe, C. (2002). Analysis of Sec22p in endoplasmic reticulum/Golgi transport reveals cellular redundancy in SNARE protein function. Mol. Biol. Cell *13*, 3314–3324.

McNew, J. A., Parlati, F., Fukuda, R., Johnston, R. J., Paz, K., Paumet, F., Söllner, T. H., and Rothman, J. E. (2000). Compartmental specificity of cellular membrane fusion encoded in SNARE proteins. Nature *407*, 153–159.

Mezzacasa, A., and Helenius, A. (2002). The transitional ER defines a boundary for quality control in the secretion of tsO45 VSV glycoprotein. Traffic *3*, 833–849.

Nemani, V. M., Lu, W., Berge, V., Nakamura, K., Onoa, B., Lee, M. K., Chaudhry, F. A., Nicoll, R. A., and Edwards, R. H. (2010). Increased expression of alpha-synuclein reduces neurotransmitter release by inhibiting synaptic vesicle reclustering after endocytosis. Neuron *65*, 66–79.

Rossi, V., Banfield, D. K., Vacca, M., Dietrich, L. E., Ungermann, C., D'Esposito, M., Galli, T., and Filippini, F. (2004). Longins and their longin domains: regulated SNAREs and multifunctional SNARE regulators. Trends Biochem. Sci. *29*, 682–688.

Rowe, T., Dascher, C., Bannykh, S., Plutner, H., and Balch, W. E. (1998). Role of vesicle-associated syntaxin 5 in the assembly of pre-Golgi intermediates. Science *279*, 696–700.

Sugeno, N., Takeda, A., Hasegawa, T., Kobayashi, M., Kikuchi, A., Mori, F., Wakabayashi, K., and Itoyama, Y. (2008). Serine 129 phosphorylation of alpha-synuclein induces unfolded protein response-mediated cell death. J. Biol. Chem. *283*, 23179–23188.

Tai, G., Lu, L., Wang, T. L., Tang, B. L., Goud, B., Johannes, L., and Hong, W. (2004). Participation of the syntaxin 5/Ykt6/GS28/GS15 SNARE complex in transport from the early/recycling endosome to the *trans*-Golgi network. Mol. Biol. Cell *15*, 4011–4022.

Tanida, I., Ueno, T., and Kominami, E. (2004). LC3 conjugation system in mammalian autophagy. Int. J. Biochem. Cell Biol. *36*, 2503–2518.

Townley, A. K., Feng, Y., Schmidt, K., Carter, D. A., Porter, R., Verkade, P., and Stephens, D. J. (2008). Efficient coupling of Sec23-Sec24 to Sec13-Sec31 drives COPII-dependent collagen secretion and is essential for normal craniofacial development. J. Cell Sci. *121*, 3025–3034.

Vogiatzi, T., Xilouri, M., Vekrellis, K., and Stefanis, L. (2008). Wild type alpha-synuclein is degraded by chaperone-mediated autophagy and macroautophagy in neuronal cells. J. Biol. Chem. *283*, 23542–23556.

Webb, J. L., Ravikumar, B., Atkins, J., Skepper, J. N., and Rubinsztein, D. C. (2003). Alpha-Synuclein is degraded by both autophagy and the proteasome. J. Biol. Chem. *278*, 25009–25013.

Xu, D., and Hay, J. C. (2004). Reconstitution of COPII vesicle fusion to generate a pre-Golgi intermediate compartment. J. Cell Biol. *167*, 997–1003.

Xu, D., Joglekar, A. P., Williams, A. L., and Hay, J. C. (2000). Subunit structure of a mammalian ER/Golgi SNARE complex. J. Biol. Chem. *275*, 39631–39639.

Yu, S., Satoh, A., Pypaert, M., Mullen, K., Hay, J. C., and Ferro-Novick, S. (2006). mBet3p is required for homotypic COPII vesicle tethering in mammalian cells. J. Cell Biol. *174*, 359–368.

Zhang, T., and Hong, W. (2001). Ykt6 forms a SNARE complex with syntaxin 5, GS28, and Bet1 and participates in a late stage in endoplasmic reticulum-Golgi transport. J. Biol. Chem. *276*, 27480–27487.